

Surface velocity in three-dimensional granular tumblers

By NICHOLAS A. POHLMAN¹, STEVEN W. MEIER²,
RICHARD M. LUEPTOW¹ AND JULIO M. OTTINO^{1,2}

¹Department of Mechanical Engineering, Northwestern University, Evanston, IL 60208, USA

²Department of Chemical and Biological Engineering, Northwestern University,
Evanston, IL 60208, USA

(Received 8 June 2005 and in revised form 5 January 2006)

A fundamental characteristic of granular flows is that they are typically restricted to thin layers of rapid surface flow. Thus, a complete understanding of surface flows is key for an accurate representation of the dynamics of the entire flow. Experiments were conducted in three-dimensional tumblers: cylindrical tumblers of various diameters, a double-cone tumbler, and a spherical tumbler, the Froude number for the last two being a function of the local geometry and ranging from 2.6×10^{-5} to 7.5×10^{-4} . Surface velocity measurements for 1 mm and 2 mm glass particles were obtained using particle tracking velocimetry. Results indicate that the streamwise surface velocity at the midpoint of the flowing layer is a linear function of local flowing layer length, regardless of tumbler shape, particle size, rotation rate, and fill fraction. In addition, the axial velocity of particles at the free surface is negligible. These results are key for the development of three-dimensional models of granular flows.

1. Introduction

Three-dimensional tumblers are used widely in industries ranging from construction to pharmaceuticals for processing granular materials. Although progress has been made in describing and characterizing granular flows (Ristow 2000; Duran 2000; Ottino & Khakhar 2000; GDR MiDi 2004), general theoretical descriptions of these flows are incomplete, and there are no fundamental governing equations. An additional complication arises in the case of polydisperse granular matter, for which the size, shape, or density are not uniform. Instead of mixing, the particles often demix, or segregate. There is, however, a characteristic of granular flows in tumblers that provides a conceptual advantage over fluid flows: the flow of granular materials in tumblers is confined to a thin region of rapid surface flow. The material below this region moves in near solid-body rotation with the tumbler, exchanging particles with the flowing layer. Thus, understanding the flow in the thin flowing layer is the key to understanding the dynamics of the entire flow.

Consider the flowing layer of thickness $\delta(x)$ in the tumbler illustrated in figure 1. The coordinate system has its origin at the midpoint of the surface of the flow with the x -axis along the streamwise direction at an angle β_m , the dynamic angle of repose, with respect to the horizontal. The y -axis is normal to the free surface and the z -axis is parallel to the axis of rotation with u , v , and w as the respective component velocities. The distance from the midpoint of the flowing layer to the tumbler wall, or half the flowing layer length, is L . The distance from the origin of the flowing

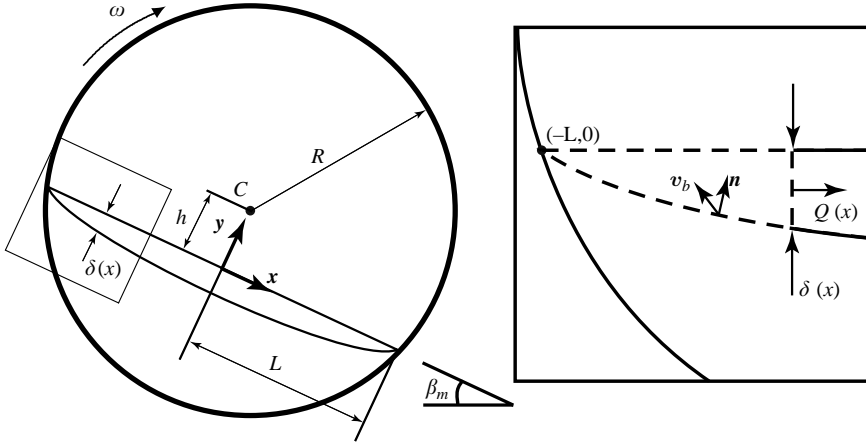


FIGURE 1. Flowing layer with angular velocity vector $\boldsymbol{\omega} = -\omega \mathbf{e}_z$. On the right is an enlargement of the upstream flowing layer.

layer to the axis of rotation, C , is given by h , and the radius of the tumbler is R . The streamwise velocity in the flowing layer decreases with depth, approaching zero at the interface of the flowing layer with the fixed bed of particles in solid-body rotation. A reasonable form for the velocity field is

$$u(x, y) = u_{\text{surf}}(x) \left(1 + \frac{y}{\delta(x)} \right)^\alpha \tag{1.1}$$

where $u_{\text{surf}}(x)$ is the streamwise surface velocity. The value of α is often set at $\alpha = 1$, based on the approximately linear velocity profile evident in quasi-two-dimensional experiments (Bonamy, Daviaud & Laurent 2002; Jain, Ottino & Lueptow 2002, 2004) and dense free-surface flow experiments (Rajchenbach 2003). The depth-averaged streamwise velocity for a given streamwise position is

$$\bar{u}(x) = \frac{1}{\delta(x)} \int_{-\delta(x)}^0 u(x, y) dy = \frac{u_{\text{surf}}(x)}{\alpha + 1}. \tag{1.2}$$

Thus, the velocity profile can be rewritten in terms of the depth-averaged streamwise velocity

$$u(x, y) = (\alpha + 1) \bar{u}(x) \left(1 + \frac{y}{\delta(x)} \right)^\alpha. \tag{1.3}$$

Particles enter/exit the flowing layer across the boundary between the flowing layer and the bed of solid-body rotation (figure 1) defined by the normal vector

$$\mathbf{n} = \frac{(\partial\delta(x)/\partial x)\mathbf{e}_x + \mathbf{e}_y}{\sqrt{1 + (\partial\delta(x)/\partial x)^2}} \tag{1.4}$$

and the velocity at which particles enter/exit the flowing layer from the bed is

$$\mathbf{v}_b = -\omega(h + \delta(x))\mathbf{e}_x - \omega x\mathbf{e}_y. \tag{1.5}$$

A mass balance equation can be written for the wedge-shaped control volume bounded by the dashed curve in the enlarged portion of figure 1. The mass flux exiting to the right, $Q(x)$, based on the bulk density, averaged streamwise velocity, and flowing layer depth, is equal to the mass flux across the fixed bed interface, $\rho_b \int \mathbf{v}_b \cdot \mathbf{n} dx$.

Assuming that the flowing layer is thin and slowly varying, $(\partial\delta(x)/\partial x)^2 \ll 1$ (which is less stringent than the assumption that $\partial\delta(x)/\partial x \ll 1$ made earlier by Khakhar *et al.* (1997)), the mass balance is

$$\rho\bar{u}(x)\delta(x) = \rho_b \int_{-L}^x \left[-\omega(h + \delta(x)) \frac{\partial\delta(x)}{\partial x} - \omega x \right] dx. \quad (1.6)$$

Assuming that to a first approximation the bulk density in the flowing layer, ρ , is similar to the bulk density in the bed, ρ_b (Jain *et al.* 2004; Orpe & Khakhar 2004), and noting that the flowing layer thickness goes to zero at the tumbler wall, $\delta(-L) = 0$, equation (1.6) can be expressed as

$$\bar{u}(x)\delta(x) = \frac{\omega}{2}[h^2 - (h + \delta(x))^2] + \frac{\omega}{2}(L^2 - x^2). \quad (1.7)$$

Since the flowing layer is thin, $\delta(x)^2/L^2 \ll 1$. Retaining only the first-order $\delta(x)$ terms, equation (1.7) yields

$$\bar{u}(x)\delta(x) = -\omega h\delta(x) + \frac{\omega}{2}(L^2 - x^2). \quad (1.8)$$

The velocity profile in the flowing layer can now be expressed as

$$u(x, y) = (\alpha + 1) \left[\frac{\omega}{2\delta(x)}(L^2 - x^2) - \omega h \right] \left(1 + \frac{y}{\delta(x)} \right)^\alpha. \quad (1.9)$$

The shear rate in the flowing layer is

$$\dot{\gamma}(x, y) = \frac{\partial u(x, y)}{\partial y} = \frac{\alpha u(x, y)}{\delta(x)} \left(1 + \frac{y}{\delta(x)} \right)^{-1}. \quad (1.10)$$

In this paper, we are primarily interested in surface flows which are at $y = 0$. Noting that $u(x, 0) = u_{\text{surf}}(x)$, equations (1.9) and (1.10) can be reduced to

$$u_{\text{surf}}(x) = (\alpha + 1) \left[\frac{\omega}{2\delta(x)}(L^2 - x^2) - \omega h \right], \quad (1.11)$$

$$\dot{\gamma}(x, 0) = \frac{\alpha u_{\text{surf}}(x)}{\delta(x)}. \quad (1.12)$$

Combining equations (1.11) and (1.12) to eliminate $\delta(x)$ and solving for $u_{\text{surf}}(x)$ yields

$$u_{\text{surf}}(x) = -\frac{(\alpha + 1)}{2}\omega h + \sqrt{\frac{(\alpha + 1)^2}{4}\omega^2 h^2 + \frac{(\alpha + 1)}{2\alpha}\omega\dot{\gamma}(x, 0)(L^2 - x^2)}. \quad (1.13)$$

For the case of a half-full tumbler, $h = 0$. Therefore, the surface velocity at the centre of the flowing layer ($x = 0$) is

$$u_{\text{surf}}(0) = L\sqrt{\frac{(\alpha + 1)}{2\alpha}\omega\dot{\gamma}(0, 0)}. \quad (1.14)$$

Thus, the surface velocity at the midpoint of the flowing layer is linearly dependent on the length of the flowing layer. Based on measurements in quasi-two-dimensional circular tumblers, α is approximately 1, resulting in the simpler expression

$$u_{\text{surf}}(0) = L\sqrt{\omega\dot{\gamma}(0, 0)}. \quad (1.15)$$

When $h \neq 0$, it can be shown that the second term under the radical in equation (1.13) is dominant since $L^2/h^2 \gg \omega/\dot{\gamma}$ and $\alpha \sim 1$ in practical situations for continuous/non-slumping flow (fill fractions greater than 10%). Thus,

$$u_{\text{surf}}(0) = -\frac{(\alpha + 1)}{2}\omega h + L\sqrt{\frac{(\alpha + 1)}{2\alpha}\omega\dot{\gamma}(0, 0)} \quad (1.16)$$

where the first term on the right-hand side accounts for the situation where the tumbler is less than half full and is small compared to the second term. Again, the streamwise surface velocity is linear with respect to the length of the flowing layer.† This result has been used as a key assumption for modelling the flow in three-dimensional tumblers (Khakhar *et al.* 1999; Gilchrist & Ottino 2003). A second assumption of these models was that the flow can be considered as independent two-dimensional slices normal to the axis of rotation (Shinbrot *et al.* 1999). In each slice, advective flow is governed by the streamwise velocity, while transverse motion is primarily diffusive with no advective component. Simulations of flows in half-filled rotating spherical tumblers using this simple model are remarkably accurate in reproducing the actual flows (Gilchrist & Ottino 2003).

Although the ‘slicing’ approach to three-dimensional modelling appears to work well, previous measurements of the velocities of granular flows in cylindrical tumblers have not directly addressed the key assumptions in the model: the dependence of the surface velocity on the length of the local flowing layer and the negligible net axial flow in the flowing layer. For flow conditions when the Froude number ($Fr = R\omega^2 g^{-1}$) is in an appropriate range, the flowing layer is continuous without intermittent avalanches and the free surface is flat (Henein, Brimacombe & Watkinson 1983; Mellmann 2001). A variety of measurement techniques have been used to measure the velocity for a continuous flat flowing layer in rotating cylindrical tumblers (magnetic resonance imaging (Nakagawa *et al.* 1993), fibre optic probes (Boateng & Barr 1997), positron emission particle tracking (Parker *et al.* 1997), video imaging (Alexander, Shinbrot & Muzzio 2002; Bonamy *et al.* 2002), and particle tracking velocimetry (Jain *et al.* 2002)); however the results focused on the streamwise surface velocity flow along the layer, $u(x, 0)$ and through the depth of the layer at the midpoint of the flowing layer, $u(0, y)$. Of particular interest here is the work of Alexander *et al.* (2002), who explored the streamwise surface velocity, $u(x, 0)$, in a rotating tumbler system based on particle tracking measurements from video images over a wide range of drum sizes and rotation rates. They found that, at low rotational speeds, the streamwise surface velocity increases in the upstream end of the flowing layer to a maximum at the midpoint of the flowing layer, and then decreases nearly symmetrically in the downstream end of the flowing layer, consistent with previous results (Boateng & Barr 1997). (At higher rotational speeds, the particles accelerate beyond the midpoint of the flowing layer resulting in a skewed streamwise velocity profile with respect to flowing layer position.) A consequence of their dimensional analysis and their measurements for different cylinder sizes and rotation rates was that, at low rotation rates for half-filled tumblers, the particle velocities are scaled by the cylinder radius, if the rotation rate is constant (Alexander *et al.* 2002). This conclusion is consistent with equation (1.14). Of course, the analysis leading to equation (1.16) indicates that the result is much more general: the streamwise surface velocity depends linearly on

† To be precise, $h = \sqrt{R^2 - L^2}$, which to a first approximation indicates that the first term in equation (1.16) is also essentially linear with L .

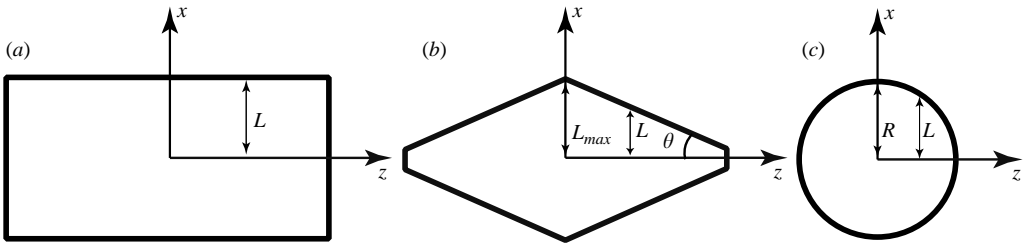


FIGURE 2. A top view schematic of the flowing layer length, L , as a function of axial position in (a) a cylinder, (b) double-cone, and (c) sphere, all rotating about the z -axis.

the length of the local flowing layer for any fill condition, regardless of tumbler radius or geometry.

The goal of this paper is to provide conclusive experimental evidence that the streamwise surface velocity scales linearly with local flowing layer length and that there is negligible axial flow in three-dimensional tumblers. The concept that the surface velocity is related to the local flowing layer length suggests that tumblers with different forms for the variation of L along the axial position, z , should be considered. We consider here the three tumbler geometries shown in figure 2. For a cylinder, L is constant for all z , but can change as a function of the fill level, since $L = \sqrt{R^2 - h^2}$. In the case of a half-full double-cone tumbler rotated about the axis of the cones, L is a linear function of axial position

$$L(z) = L_{max} - |z| \tan \theta \quad (1.17)$$

where L_{max} is the maximum radius at the centre of the double-cone ($z = 0$), and θ is half the opening angle of the cone. (Note that this geometry is different from industrial double-cone blenders, examples of which have been studied extensively (Alexander, Shinbrot & Muzzio 2001), where the rotation axis is perpendicular to the axis of the cones to induce time-periodicity for improved mixing performance.) For the case of a half-full spherical tumbler, L for each cross-section is equal to one-half the length of the chord so that L varies nonlinearly with axial location as

$$L(z) = \sqrt{R^2 - z^2} \quad (1.18)$$

where $z = 0$ is at the centre of the sphere.

In this work, we present results of measurements of the surface velocity in all three cases to examine (i) the degree to which the streamwise velocity at the surface depends on the flowing layer length and (ii) the nature of the axial flow at the surface. The investigation is limited to continuous flow with an essentially flat free surface, represented by local Froude numbers ($Fr(z) = L(z)\omega^2 g^{-1}$) in the range of 2.6×10^{-5} to 7.5×10^{-4} . In this range of Froude numbers, the surface remains flat and the flattening and/or skewing of the velocity profile along the flowing layer length is minimal (Alexander *et al.* 2002).

2. Experimental methods

Particle tracking velocimetry (PTV) was used to measure surface velocity. In order to obtain images of the flowing free surface in the three tumbler geometries without optical distortion due to the curved tumbler wall, a 90° wedge was cut out of each tumbler, as shown schematically in figure 3. The rotation of the tumbler was controlled

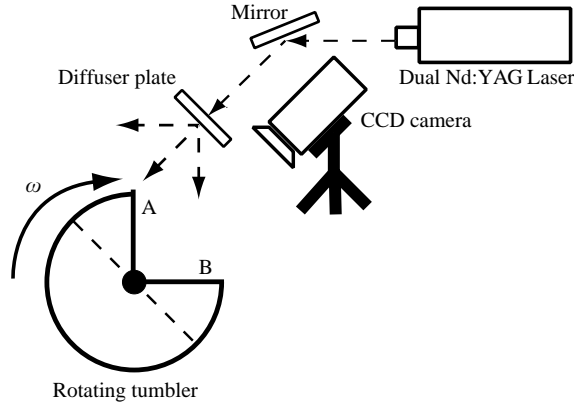


FIGURE 3. A schematic of the experimental set-up which includes the rotating tumbler, the CCD camera to record particle locations, the Nd:YAG laser light source, a re-directing mirror, and a diffuser plate.

with a DC stepper motor. The container was first rotated counter-clockwise such that edge A of the cut-out was nearly parallel to the surface of the granular material, which had a static angle of repose, β_s , ranging from 20° to 24° . Images of the flowing free surface were recorded as the system rotated clockwise. Rotation and image acquisition were stopped just before the material poured out over the edge B of the cut-out.

To maintain similar conditions for the cylinder, double-cone, and spherical tumblers, the maximum diameter for all cases was nearly the same, 13.6 to 14.0 cm. The cylindrical tumbler was a 17.5 cm long acrylic tube with an internal diameter of 14.0 cm and having acrylic endwalls. Cylindrical tumblers of diameters 7.0, 10.0, and 17.0 cm and lengths of 17.5 cm were also used. The conical tumbler was made of two high-density polyethylene funnels with an opening angle of 60° and a maximum diameter of 13.8 cm joined with RTV silicone to form the double-cone. The narrow ends of the cones were truncated at a diameter of 2.1 cm ($z = \pm 9.6$ cm) with aluminium plugs. The spherical tumbler was constructed of two moulded plastic hemispheres with a diameter of 13.6 cm. All tumblers were wiped with a de-static agent prior to operation to reduce electrostatic effects on the particle flow.

The tumblers were typically filled to 50% volume fraction with one of the two particle types: 1.07 ± 0.04 mm black basalt glass beads ($\rho = 2.6 \text{ g cm}^{-3}$) or 2.07 ± 0.06 mm silica glass beads coated with black enamel paint ($\rho = 2.3 \text{ g cm}^{-3}$). The particles were illuminated by a 25 mJ Nd:YAG laser (New Wave Research) synchronized with a 1 megapixel charged coupled device (CCD) camera (TSI) to obtain images. The camera was positioned such that the focal plane was at the dynamic angle of repose of the flowing material, $\beta_m = 23^\circ$ – 30° depending upon the tumbler and particle size. The laser beam was directed normal to the face of the diffuser plate, which was held in a fixed position and tilted at the dynamic angle of repose for the particle size and tumbler combination. The position of the illumination and camera, along with the black colour of the beads, provided optimal visibility for locating the bead positions by virtue of a single bright spot of reflected laser light on each bead with an otherwise black background.

Image pairs separated by $\Delta t = 1.5$ ms were obtained at the rate of 15 Hz. The image pairs were first analysed using particle image velocimetry software (*Insight*, TSI) to obtain an estimate of the velocity of the particles at the free surface. From

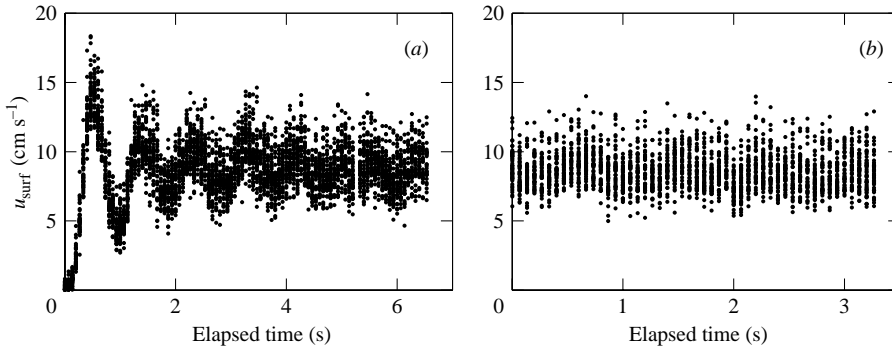


FIGURE 4. Velocity of the free surface as a function of time for 1 mm particles rotated at 2 r.p.m. in a 14.0 cm diameter cylinder. (a) Measurement started with the free surface poised at the angle of repose. (b) A typical steady-state measurement.

these results, PTV was used to measure the velocities of individual particles (Cowen & Monismith 1997; Jain *et al.* 2002). Errors due to the location of the bright spot on a particle were at most 1 pixel. This error potentially contributes a bias to the velocity of less than 0.5%. The positions of particles in each image were identified to sub-pixel resolution, resulting in an error of less than 2% in the velocity for individual particles.

The typical field of view for the image was 2.5–4.3 cm depending upon the particle size as well as how close the camera could be positioned to the free surface without interfering with the tumbler. A traverse was used to move the camera in the axial direction allowing the image sets to be pieced together to give a full axial representation of the free-surface velocity field. The velocities of particles within one particle diameter of the axis of rotation ($x = 0$) were sorted into three-particle-diameter wide bins along the axial direction in order to calculate a local mean and standard deviation. The standard deviation levelled off when at least fifty image pairs were ensemble-averaged, so a total of 100 image pairs were used at each measurement location. The bins typically contained 200 or more particle velocity measurements, of which vectors that were more than five standard deviations away from the mean were ignored, eliminating no more than 0.1% of the total vectors available from PTV.

The tumbler could only be rotated a limited angle before the beads spilled out of the cut-out. As a result, it was necessary to determine when the start-up transient effects of the granular flow had decayed so that the data represented steady-state behaviour. Tests were conducted to determine the transient dynamics of the free surface poised at the static angle of repose starting from rest. A typical result of a single trial in which the rotation starts with the material poised at the static angle of repose is shown in figure 4(a) where the streamwise component of all of the vectors within one particle diameter of the axis of rotation are shown as a function of time. The overall form of the transient dynamics of the surface velocity are evident. The velocity peak at approximately 0.5 s is due to a large avalanche at the angle of marginal stability. Successively decaying oscillations are due to second and third avalanches, with the surface material moving at near steady velocity after several oscillations. The results presented here are for steady flow after the oscillations had decayed and before the tumbler reached the rotation limit of the cut-out. A typical example of a steady-state measurement is shown in figure 4(b). In these cases, the tumbler rotation began before the free surface reached the static angle of repose, reducing the amplitude and

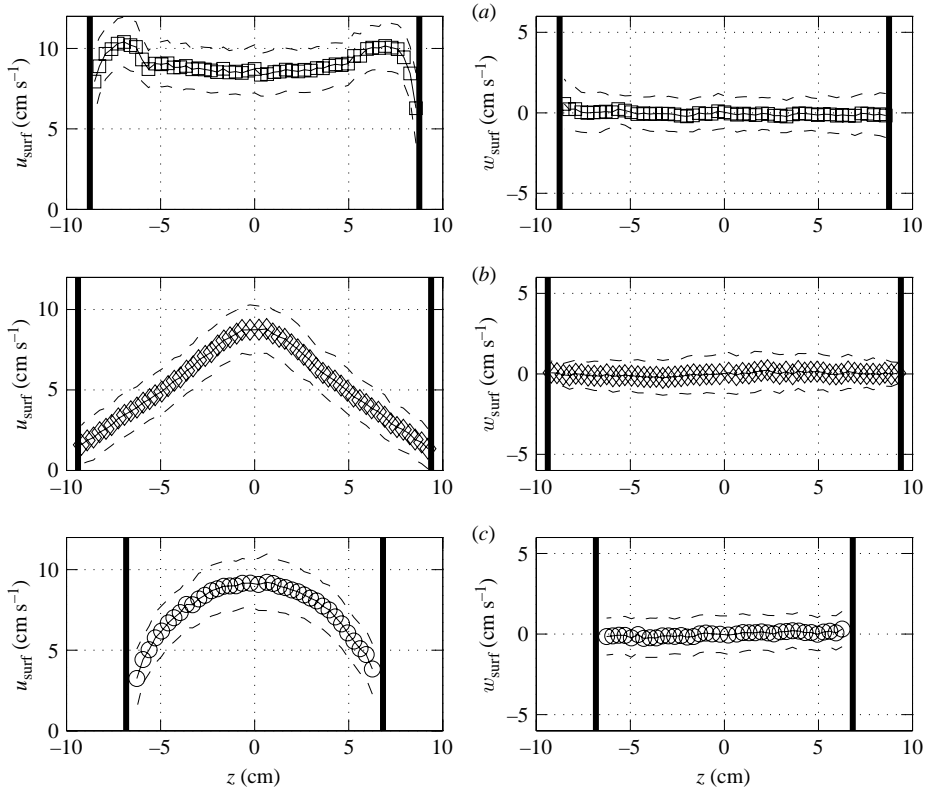


FIGURE 5. The streamwise (left) and axial (right) surface velocity for 1 mm particles at the midpoint of the flowing layer as a function of the axial position in all tumblers: (a) \square , cylinder; (b) \diamond , double-cone; (c) \circ , sphere; the dark vertical lines indicate endwalls. The solid curve with symbols is the mean velocity. The dashed curve is one standard deviation above and below the mean velocity.

duration of the oscillations compared to that shown in figure 4(a). Each individual trial was verified to have negligible oscillation of the streamwise velocity component to assure steady-state conditions in all cases.

3. Results

Surface velocity profiles for 50% fill fraction with 1 mm particles rotated at 2.0 r.p.m. are shown in figure 5 for the cylinder (a), double-cone (b), and sphere (c). The left column shows the streamwise velocity component, u_{surf} , while the right column gives the axial velocity, w_{surf} . Similar velocity profiles were observed for 2 mm particles, shown in figure 6. Velocities near the left endwall of the cylinder for 2 mm particles could not be recorded due to a shadow being cast by the endwall.

Consider first the 14.0 cm cylindrical tumbler. The streamwise velocity u_{surf} is approximately 8.7 cm s^{-1} for 1 mm particles in the centre of the tumbler with negligible net axial velocity w_{surf} , and a very small reduction of streamwise velocity to approximately 8.1 cm s^{-1} for 2 mm particles with the similar negligible net axial velocity. The streamwise velocity profile is symmetric along the axial direction of the cylinder with the slowest velocity near the endwalls, consistent with the reduction in

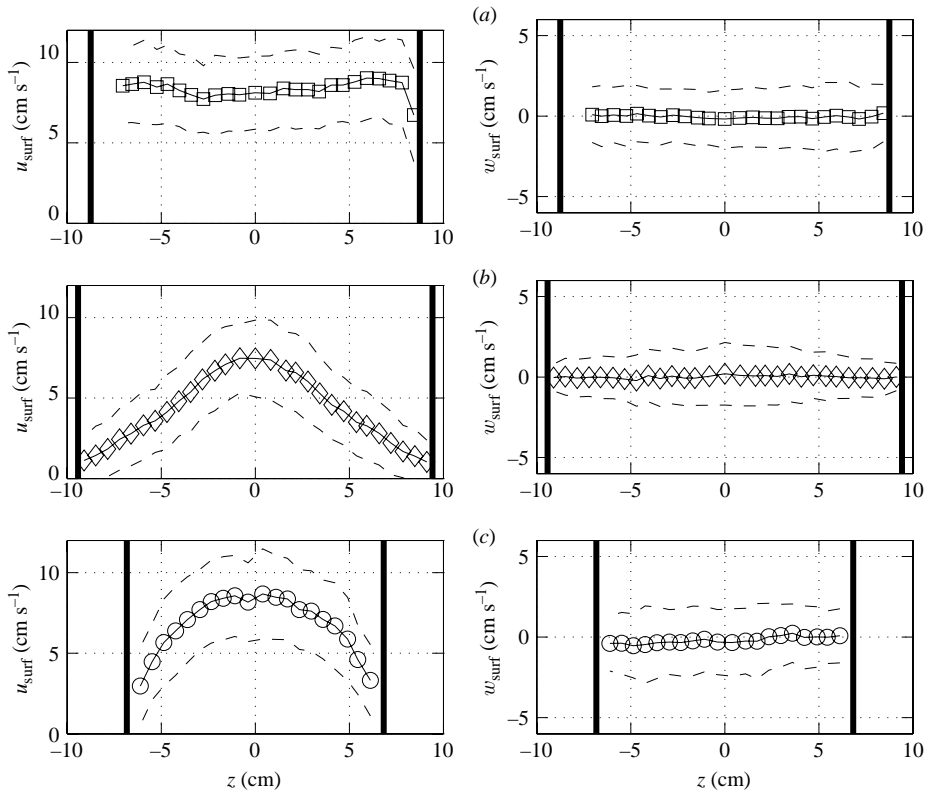


FIGURE 6. The streamwise (left) and axial (right) surface velocity for 2 mm particles at the midpoint of the flowing layer as a function of the axial position in (a) cylinder, (b) double-cone and (c) spherical tumblers. Symbols are the same as figure 5.

velocity near a sidewall that occurs in chute flow (Ahn, Brennen & Sabersky 1991; Jop, Forterre & Pouliquen 2005) and rotating tumblers (Maneval *et al.* 2005).

The velocity is 17% higher a short distance from the endwalls than at the centre of the cylinder for 1 mm particles (11% for 2 mm), an effect that has previously been observed experimentally (Boateng & Barr 1997) and conjectured from mixing tests (Santomaso, Olivi & Canu 2004). Friction between particles and the endwall slows the streamwise flow of particles adjacent to the endwalls. However, due to conservation of mass, all of the particles in the fixed bed must pass through the flowing layer every half-revolution for a half-full tumbler and more frequently for lower fill levels. Although the axial velocity at the midpoint of the flowing layer is negligible (as shown in figures 5 and 6), particles apparently flow away from the wall in the upstream region of the flowing layer and back toward the wall in the downstream region of the flowing layer, so that there is a fast-flowing region 2–3 cm from the endwall.

The streamwise velocity for the double-cone tumbler is maximum at the centre, where the diameter is largest (figures 5*b* and 6*b*). The streamwise velocity decreases linearly as a function of the axial position, corresponding to the linear decrease in the local flowing layer length of the two cones. In the spherical tumbler, the maximum streamwise velocity occurs at the centre, where the flowing layer length is greatest, and then decreases nonlinearly with axial position as the flowing layer length decreases

Particle size	1 mm		2 mm	
	σ_u	σ_w	σ_u	σ_w
Cylinder	1.4 ± 0.2	1.1 ± 0.1	2.4 ± 0.1	1.8 ± 0.1
Double-cone	1.4 ± 0.1	1.0 ± 0.2	2.1 ± 0.3	1.5 ± 0.3
Sphere	1.6 ± 0.09	1.1 ± 0.06	2.6 ± 0.2	2.0 ± 0.2

TABLE 1. The standard deviation σ for both particle sizes of the component velocity averaged over the axial length of the tumblers in cm s^{-1} .

(figures 5c and 6c). In both cases, the axial velocity of the free surface is very close to zero.

The higher streamwise velocity near the endwalls that was evident in the cylindrical tumbler was not observed in the double-cone and sphere for two reasons. First, due to the geometric shape of the sphere and double-cone tumblers, the ‘endwalls’ have negligible area and thereby presumably little frictional effect on the streamwise velocity. Second, the length of the flowing layer decreases to near zero at the axial extremes of these tumblers so that the surface velocity is negligible here regardless of frictional effects (equation (1.16)).

The standard deviations σ_u and σ_w of the streamwise and axial velocities (the dashed curves in figures 5 and 6) are reported in table 1 for both particle sizes and the three tumbler geometries tested. The standard deviation indicates the degree of diffusion that occurs as particles pass through the flowing layer. Given the similar magnitudes of the standard deviation for each geometry, it appears that changing the container shape does not significantly affect the degree of streamwise or axial diffusion in the surface flow of the tumbler. Furthermore, the skewness of the axial velocity was less than ± 0.5 with no dependence on the axial position in all three tumbler geometries, indicating that axial diffusion does not have a preferred direction (individual particle axial velocity components are evenly distributed about the mean), regardless of the shape of the tumbler. However, axial diffusion is clearly related to the particle size for all tumbler shapes as would be expected from simple scaling arguments. Also, diffusion appears to be anisotropic. The streamwise diffusion as reflected by the velocity fluctuations is somewhat larger than the axial diffusion at the surface of the flowing layer.

The maximum streamwise velocity shown in figures 5 and 6 is similar for all three tumblers and corresponds to the location of the maximum dimension of the tumbler, which is nearly the same for all tumblers. This similarity suggests that the local streamwise velocity is indeed related to the local flowing layer length as predicted by equation (1.16). The relationship is shown more clearly in figure 7 where results for all three tumbler geometries are superimposed for both tested particle sizes. The range of values of the streamwise velocity at $L = 7$ cm for the 14.0 cm diameter cylinder reflects the variation in the streamwise velocity with axial position (including the high-velocity regions near the endwalls but excluding the data immediately adjacent to the endwalls). Also shown in the plot for the 1 mm particles in figure 7(a) are the streamwise velocities for 7.0 cm, 10.0 cm, and 17.0 cm diameter cylinders for which L is 3.5 cm, 5.0 cm, and 8.5 cm, respectively. The streamwise velocity has a range of values in these cases, but the midpoint of that range clearly exhibits the same linear relationship as the values for the other tumblers having maximum flowing layer lengths of about $L = 7.0$ cm. Finally, the data for $L = 7.75$ cm were obtained

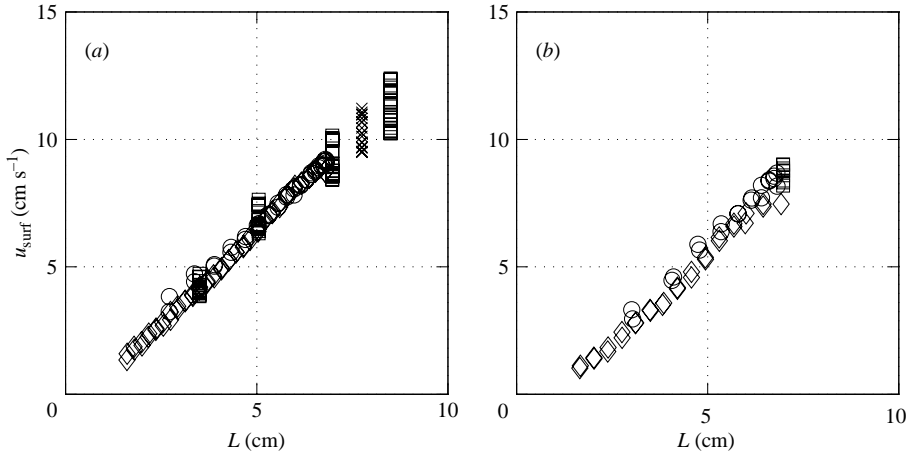


FIGURE 7. The local streamwise surface velocity as a function of the local flowing layer length at a rotation rate of 2.0 r.p.m.: \square , cylinder; \diamond , double-cone; \circ , sphere; \times , 25% full cylinder. Particle sizes are (a) 1 mm and (b) 2 mm.

in the 17.0 cm diameter cylinder with $h = 3.5$ cm (fill level of approximately 25%). (Equation (1.16) is valid here since the ratio L^2/h^2 is 4.9, which is much greater than the ratio of $\omega/\dot{\gamma}$, given that ω is $O(0.1)$ and $\dot{\gamma}$ is $O(10)$). In this case, the initial velocity of the particles entering the flowing layer is not perpendicular to the free surface as in the case for a half-full tumbler, making the first term on the right-hand side of equation (1.16) non-zero. Therefore, the velocity plotted at $L = 7.75$ cm in figure 7(a) was adjusted by adding ωh (assuming $\alpha = 1$) to the measured surface velocity. Results for all three tumblers with 2 mm particles have nearly the same dependence of streamwise velocity on the flowing layer length as shown in figure 7(b). The important point that can be extracted from figure 7 is the clear linear dependence of the streamwise velocity on the local length of the flowing layer, just as predicted by equation (1.16), regardless of the tumbler geometry, tumbler diameter, fill level, or particle size.

Equation (1.15) indicates that the slope of the data in figure 7 should be related to the shear rate. Using this relationship, the theoretical shear rate at 2.0 r.p.m. can be estimated as 9.3 s^{-1} for the sphere and 10.3 s^{-1} for the double-cone for 1 mm particles, while the estimated shear rate for 2 mm particles is 9.8 s^{-1} for the sphere and 8.8 s^{-1} for the double-cone. (This estimate is difficult to make for the cylinders, because there is only a single flowing layer length for each cylindrical tumbler instead of a range of flowing layer lengths, as for the double-cone and spherical tumblers.) Additional experiments were conducted at different rotation rates using the 1 mm particles and all tumbler geometries. The varying rotation rates produce velocity profiles and standard deviations similar to those shown in figures 5 and 6. Nonetheless, as shown in figure 8(a), each rotation rate exhibits a linear relationship between the streamwise surface velocity and the flowing layer length. It is tempting to try to collapse the data by assuming that $\dot{\gamma}(0, 0)$ and α in equation (1.14) are constant for all tumbler geometries and rotation rates and by plotting u_{surf} as a function of $\sqrt{\omega}L$, shown in figure 8(b). Although there is a tendency toward collapse, the collapse is imperfect because of the range of shear rates: 8.7, 9.8, 11.5, and 12.2 s^{-1} for 1.5, 2.0, 2.5, and 3.0 r.p.m., respectively (estimated from each data set at a particular rotation rate using equation (1.15)). Thus, the shear rate $\dot{\gamma}(0, 0)$ is a weak function of rotation rate. This

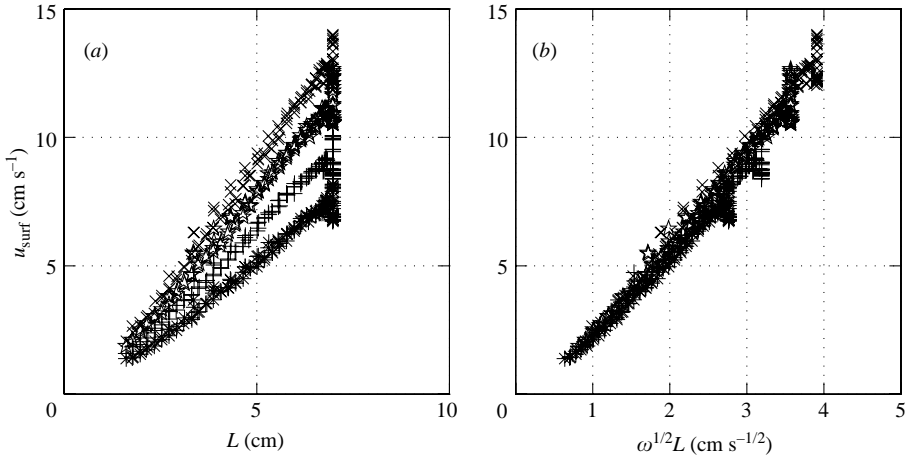


FIGURE 8. The local streamwise surface velocity for different rotation rates as a function of: (a) the local flowing layer length; (b) the local flowing layer length scaled by the square root of rotation rate. Rotation rates are: *, 1.5 r.p.m.; +, 2.0 r.p.m.; ★, 2.5 r.p.m.; ×, 3.0 r.p.m. Particle size is 1 mm and all tumbler geometries with a maximum diameter of 13.6 cm to 14.0 cm are represented.

is consistent with existing theory, which indicates that shear rate is indirectly related to the rotation rate (Khakhar *et al.* 2001). This theory estimates the shear rate as

$$\dot{\gamma}(0, 0) = \left[\frac{g \sin(\beta_m - \beta_s)}{cd \cos \beta_s} \right]^{1/2} \quad (3.1)$$

where g is acceleration due to gravity, c is an empirical fitting parameter, d is the particle diameter, β_s is the static angle of repose, and β_m is the dynamic angle of repose. Since β_m is a function of rotation rate, the shear rate must depend on the rotation rate. However, it is quite difficult to directly relate the shear rate estimated from figures 7 or 8 to the prediction of equation (3.1). The values of β_s and β_m are difficult to measure accurately in the apparatus shown in figure 3, and equation (3.1) is quite sensitive to the values of β_s and β_m . In addition, the value of the empirical fitting parameter c is based on quasi-two-dimensional tumblers (Orpe & Khakhar 2001). The value of c has not been determined for flow in three-dimensional tumblers, and it is likely that it differs substantially from the value for quasi-two-dimensional tumblers due to endwall effects.

4. Conclusions

The fundamental nature of granular flow in thin shear layers suggests that the assumption of a relationship between surface velocity and flowing layer length is a useful approach to modelling granular flows in three-dimensional tumblers (Gilchrist & Ottino 2003). Alexander *et al.* (2002) indicated that streamwise particle velocities are scaled by the radius in half-full cylinders. Our work expanded this idea based on the theoretical relationship of equation (1.16) that the magnitude of the local streamwise surface velocity is a linear function of the local flowing layer length, and we showed that the concept is valid despite significant variations in the tumbler shape, tumbler size, particle size, rotation rate, and fill fraction. Furthermore, there is negligible net axial motion at the midpoint of the flowing layer for all tumblers.

However axial flow has been observed in the upstream and downstream portions of the flowing layer near the perpendicular endwalls of a cylindrical tumbler. The standard deviation of the axial velocity in three-dimensional tumblers is independent of axial position, which suggests that axial diffusion is not affected by the shape of the tumbler, the flowing layer length, or the axial gradients of the streamwise velocity.

The results reported in this paper are limited to steady continuous flat free-surface flow of granular particles for tumblers in which the flowing layer length changes smoothly with respect to axial position. Clearly this work suggests other areas of investigation. Of particular interest is the higher streamwise velocity near the endwalls of cylindrical tumblers and the axial velocity components of particles upstream and downstream of the midpoint of the flowing layer. In addition, changes in the flowing layer depth along the axis of rotation may be related to the observed increase in streamwise velocity near the endwalls. In fact, it has not escaped our attention that given the relationship between $u_{\text{surf}}(x)$ and $\delta(x)$ in equation (1.11), the flowing layer depth at the midpoint, $\delta(0)$, can be predicted from the measurement of u_{surf} . For a 50% fill fraction and assuming $\alpha = 1$, $\delta(0)$ can be estimated to range from 0.3 cm for $L = 2$ cm to 1.2 cm for $L = 8$ cm. However, the nature of the experimental apparatus did not permit confirming these estimates of the flowing layer thickness. Another interesting phenomenon observed was a series of avalanches of decaying amplitude in the initial flow upon start-up. Further investigation of the transient character of flow prior to steady-state motion may provide insight into other flow regimes.

Two other issues, more speculative, should be mentioned to point out avenues for future investigations. One is the influence of particle diameter on shear rate and diffusion. Theoretical guidance in this case is limited. The theory developed by Khakhar, Orpe & Ottino (2001) suggests that the shear rate should be proportional to $d^{-1/2}$ as indicated in equation (3.1). Our data, however, cover only two particle diameters. More data are needed before firm conclusions can be extracted about the effect of particle size. The second issue is whether the standard deviation of the streamwise and axial velocity fluctuations, σ , which are the same order of magnitude, can be somehow connected to collisional diffusivity, D , via σ times a characteristic length such as the particle diameter, d . If this is the case, using Savage's relationship of D being proportional to $d^2\dot{\gamma}$ (Savage 1993), we conclude that σ should scale as $d\dot{\gamma}$ as appears to be the case to a first approximation when comparing σ for 1 mm and 2 mm particles (table 1), though more data are needed. Finally, the limitations of the linear relationship of streamwise velocity with flowing layer length should be explored. For instance, the surface velocity may approach an asymptotic value when the flowing layer length becomes large enough, or the surface velocity may have a different dependence on flowing layer length when a skewed velocity profile occurs at higher tumbler rotation rates (Alexander *et al.* 2002).

This work was funded in part by the Office of Basic Energy Sciences of the Department of Energy (DE-FG02-95ER14534) and by the National Science Foundation IGERT Program "Dynamics of Complex Systems in Science and Engineering" (DGE-9987577). S. W. Meier was also funded by a National Science Foundation Graduate Research Fellowship.

REFERENCES

- AHN, H., BRENNEN, C. E. & SABERSKY, R. H. 1991 Measurements of velocity, velocity fluctuation, density, and stresses in chute flows of granular materials. *J. Appl. Mech.* **58**, 792–803.

- ALEXANDER, A., SHINBROT, T. & MUZZIO, F. J. 2002 Scaling surface velocities in rotating cylinders as a function of vessel radius, rotation rate, and particle size. *Powder Technol.* **126**, 174–190.
- ALEXANDER, A. W., SHINBROT, T. & MUZZIO, F. J. 2001 Granular segregation in the double-cone blender: Transitions and mechanisms. *Phys. Fluids* **13**, 578–587.
- BOATENG, A. A. & BARR, P. V. 1997 Granular flow behaviour in the transverse plane of a partially filled rotating cylinder. *J. Fluid Mech.* **330**, 233–249.
- BONAMY, D., DAVIAUD, F. & LAURENT, L. 2002 Experimental study of granular surface flows via a fast camera: A continuous description. *Phys. Fluids* **14**, 1666–1673.
- COWEN, E. A. & MONISMITH, S. G. 1997 A hybrid digital particle tracking velocimetry technique. *Exp. Fluids* **22**, 199–211.
- DURAN, J. 2000 *Sands, Powders, and Grains: An Introduction to the Physics of Granular Materials*. Springer.
- GDR MiDI 2004 On dense granular flows. *Eur. Phys. J. E* **14**, 341–365.
- GILCHRIST, J. F. & OTTINO, J. M. 2003 Competition between chaos and order: Mixing and segregation in a spherical tumbler. *Phys. Rev. E* **68**, 061303.
- HENEIN, H., BRIMACOMBE, J. K. & WATKINSON, A. P. 1983 Experimental study of transverse bed motion in rotary kilns. *Metall. Trans. B* **14B**, 191–205.
- JAIN, N., OTTINO, J. & LUEPTOW, R. M. 2002 An experimental study of the flowing granular layer in a rotating tumbler. *Phys. Fluids* **14**, 572–582.
- JAIN, N., OTTINO, J. M. & LUEPTOW, R. M. 2004 Effect of the interstitial fluid on a flowing granular layer. *J. Fluid Mech.* **508**, 23–44.
- JOP, P., FORTERRE, Y. & POULIQUEN, O. 2005 Crucial role of side walls for granular surface flows: consequences for the rheology. *J. Fluid Mech.* **541**, 167–192.
- KHAKHAR, D. V., MCCARTHY, J. J., GILCHRIST, J. F. & OTTINO, J. M. 1999 Chaotic mixing of granular materials in two dimensional tumbling mixers. *Chaos* **9**, 195–205.
- KHAKHAR, D. V., MCCARTHY, J. J., SHINBROT, T. & OTTINO, J. M. 1997 Transverse flow and mixing of granular materials in a rotating cylinder. *Phys. Fluids* **9**, 31–43.
- KHAKHAR, D. V., ORPE, A. V. & OTTINO, J. M. 2001 Surface granular flows: two related examples. *Adv. Complex Syst.* **4**, 407–417.
- MANEVAL, J. E., HILL, K. M., SMITH, B. E., CAPRIHAN, A. & FUKUSHIMA, E. 2005 Effects of endwall friction in rotating cylinder granular flow experiments. *Granular Matter* **7**, 199–202.
- MELLMANN, J. 2001 The transverse motion of solids in rotating cylinders – forms of motion and transition behavior. *Powder Technol.* **118**, 251–270.
- NAKAGAWA, M., ALTOBELLI, S. A., CAPRIHAN, A., FUKUSHIMA, E. & JEONG, E.-K. 1993 Non-invasive measurements of granular flows by magnetic resonance imaging. *Exp. Fluids* **16**, 54–60.
- ORPE, A. V. & KHAKHAR, D. V. 2001 Scaling relations for granular flow in quasi-two-dimensional rotating cylinders. *Phys. Rev. E* **64**, 031302.
- ORPE, A. V. & KHAKHAR, D. V. 2004 Solid-fluid transition in a granular shear flow. *Phys. Rev. Lett.* **93**, 068001.
- OTTINO, J. M. & KHAKHAR, D. V. 2000 Mixing and segregation of granular materials. *Annu. Rev. Fluid Mech.* **35**, 55–91.
- PARKER, D. J., DIJKSTRA, A. E., MARTIN, T. W. & SEVILLE, J. P. K. 1997 Positron emission particle tracking studies of spherical particle motion in rotating drums. *Chem. Engng Sci.* **52**, 2011–2022.
- RAJCHENBACH, J. 2003 Dense, rapid flows of inelastic grains under gravity. *Phys. Rev. Lett.* **90**, 144302.
- RISTOW, G. H. 2000 *Pattern Formation in Granular Materials* Springer.
- SANTOMASO, A., OLIVI, M. & CANU, P. 2004 Mechanisms of mixing of granular materials in drum mixers under rolling regime. *Chem. Engng Sci.* **59**, 3269–3280.
- SAVAGE, S. B. 1993 Disorder, diffusion and structure formation in granular flow. In *Disorder and Granular Media* (ed. D. Bideau & A. Hansen), pp. 255–285. Elsevier.
- SHINBROT, T., ALEXANDER, A., MOAKHER, M. & MUZZIO, F. J. 1999 Chaotic granular mixing. *Chaos* **9**, 611–620.